Space Shuttle Solid Rocket Motor Plume Pressure and Heat Rate Measurements

Wulf von Eckroth,* Leah Struchen,† Thomas Trovillion,‡ Rafael Perez,† and Shaun Nerolich§
United Space Alliance, Kennedy Space Center, Florida 32780
and
Chris Parlier¶
NASA, Kennedy Space Center, Florida 32899

The solid rocket booster main flame deflector at NASA Kennedy Space Center Launch Complex 39A was instrumented to measure heat rates, pressures, and temperatures on the final three space shuttle launches. Because the solid rocket booster plume is hot and erosive, a robust tungsten piston calorimeter was developed to compliment measurements made by off-the-shelf sensors. Witness materials were installed, and their melting and erosion response to the Mach 2, 4000°F, 4 s duration plume was observed. The data show that the specification used for the design of the main flame deflector thermal protection system overpredicts heat rates by a factor of three and underpredicts pressures by a factor of two. The discovery of short-duration heating spikes that occur when aluminum oxide slag solidifies on the main flame deflector explains this heat rate overprediction. This study allows improvement of solid rocket motor launch site and test stand computational fluid dynamics models and the concomitant slag deposition heat transfer models.

Nomenclature

c_v = specific heat, $Btu/lb_m \cdot °F$
k = thermal conductivity, $Btu/ft \cdot h \cdot °F$
T = temperature, °F
x = distance or depth, in.
α = thermal diffusivity, ft^2/h
ΔH_f = heat of fusion, Btu/lb_m
ρ = density, lb_m/ft^3

I. Introduction

ALMOST all launch facilities and test stands in the world use flame deflectors to redirect rocket motor exhaust plumes away from the ground based infrastructure. The main flame deflectors (MFDs) installed at NASA Kennedy Space Center (KSC) Launch Complex 39 (LC-39) were used for the space shuttle and are intended for use in future space programs. These flame deflectors are covered with refractory concrete. This refractory concrete is used at launch facilities world-over including Stennis Space Center, Cape Canaveral Air Force Station, Vandenberg Air Force Base, Wallops Flight Facility, and Guiana Space Centre. At KSC, it is used on both sides of the deflector: the main engine side and the solid rocket booster (SRB) side. Damage has primarily occurred on the SRB side, cracking and shattering at liftoff, releasing foreign object debris. The liberation of refractory concrete is both expensive to repair and potentially damaging to ground support equipment. Figure 1b illustrates some of the major LC-39A ground structures, including the MFD located directly beneath the space shuttle SRBs. Because refractory concrete on the MFD has very little tensile strength, pieces of this material weighing over 80 lb have liberated, flying hundreds of feet to strike and damage ground support equipment. The expensive process of reapplying refractory concrete has become a regular part of the pad refurbishment process after each launch. Figure 1a shows the SRB plume shortly after liftoff of STS-135 and illustrates the two types of fluids causing the extreme environment affecting the MFD. The brownish colored clouds to the sides of the photograph are SRB combustion exhaust, and the gray clouds in the center foreground are water vapor from the sound suppression system and space shuttle main engine exhaust.

Although refractory concrete is held to the substrate of the steel deflector by grid steel and steel studs, elimination of foreign object debris was largely unsuccessful using mechanical systems. The Mach 2, 4000°F, SRB plume causes erosion of the refractory concrete and exposes the steel studs to the severe environment published in NASA Technical Standard GP-1059 [1]. This standard documents the environmental loads on pad structures and was generated from numerical models. Microstructural analysis on the steel studs discovered no signs of melting [2]. When the loads documented in GP-1059 are used as input to a thermal model, the exposed steel is predicted to melt. The anecdotal evidence does not support the output of the thermal models generated using GP-1059 input loads. It was questioned whether refractory concrete was necessary to protect the steel substrate of the MFD or if a better material could be used. The pressure and heat rate environments on ground support equipment in the vicinity of the SRB plume have been studied numerous times, as documented in publications such as "Testing Requirements for Refractory Concrete" [3] and NASA DD-818-TR [4]. However, these studies involved instrumenting the side flame deflector or the flame trench wall, panels orthogonal to the SRB plume flow. These are relatively benign environments compared with a surface impinged upon directly by the plume. Before this study, the loads beneath the plume on the MFD had never been measured.

As next-generation space programs such as the space launch system are developed, computational fluid dynamics models are an increasingly important tool used to generate comprehensive

*Launch Site Design Manager, Engineering Project Management, USK-800. Senior Member AIAA.
†Staff Engineer, Strength and Thermal Analysis Department, USK-841. Professional Member AIAA.
‡Senior Staff Engineer (retired), Technical Analysis Department. Senior Member AIAA.
§Staff Engineer, Loads and Dynamics Analysis Department, USK-841. Senior Member AIAA.
¶Staff Engineer, Mechanical Support Systems Engineering Branch, Mail Stop NE-M6.

a) STS-135 SRB plume   **b) Space shuttle and the main flame deflector**

Fig. 1   Space shuttle launch complex LC-39A.

understanding of the environment. These models provide great detail, but given the complicated nature of the flow and the assumptions required within the models their accuracy can only be determined by how they agree with measured data. This study acquired data at selected sites on the MFD. Localized pressure, heat rate, and material response data were acquired and can be used for reality checks at the location of the sensors in the models. In addition, steel witness rods were installed in close proximity to the sensors to gather qualitative evidence of the environment.

II.   MFD Instrumentation Site Selection

The refractory concrete along the entire bottom and west (right) side of the deflector displayed very low compressive strengths, as seen in Fig. 2. When cored specimens were tested from the west side after STS-125 in May 2009, one sample demonstrated a compressive strength as low as 416 psi with an average of 1770 psi. The specification [5] for refractory concrete stipulates a compressive strength of 4500 psi at 7 days. Tensile stresses within the refractory concrete are complex and are induced from flexure and vibration of the MFD during launch. Because the tensile strength of the refractory concrete was determined to be less than 10% of the compressive strength [6], it can be seen that low strengths in this material will result in cracking and liberation during the launch event. The slope at the bottom of the MFD experiences some of the worst erosion because it physically turns the plume from vertical to horizontal. The west and bottom areas of concrete were replaced before STS-133 in January 2011 because of their low strength and high foreign object debris risk. The MFD before this refurbishment is described further in Sec. V.E.

A new refractory concrete installation technique was developed using casting to replace the historic gunning technique in order to improve MFD strength. The water-to-cement ratio in refractory concrete greatly influences its compressive strength, and the casting technique better controls the water-to-cement ratio. Furthermore, measurements returned from instrumentation installed flush with the MFD face, within the boundary layer, are dependent on the smoothness of the surface. The formwork left a smooth faceted surface with 0- to 1/2-in.-high horizontal ridges as a result of using

2-in.-thick by 12-in.-wide form boards. This cast surface was deemed acceptable for obtaining these measurements.

Three areas along the west side of the MFD were selected for sensor installation during the concrete refurbishment process based on GP-1059 data. One "sensor suite" installed in each of the three sites is further described in Sec. III as made up of one tungsten piston calorimeter (TPC), one commercial-off-the-shelf (COTS) sensor set, and one witness rod. Figure 3 presents the plan view of the heat rate contours for the SRB exhaust impingement on the MFD at 1 s after SRB ignition [defined as mission elapsed time (MET) of +1 s]. Directly beneath the SRBs, the very dense contours indicate that a distance of less than 10 ft separates the heat rates of 5000 and 1000 Btu/ft$^2 \cdot$ s. To capture the governing heat rate, one sensor suite was installed as close as possible to the "K" central contour. The uppermost sensors were actually installed near the "H" contour, based on access from the backside of the MFD and spacing of the steel structural stiffeners. Two additional sensor suites were installed downhill from the upper set, as illustrated in Fig. 4. Additionally,
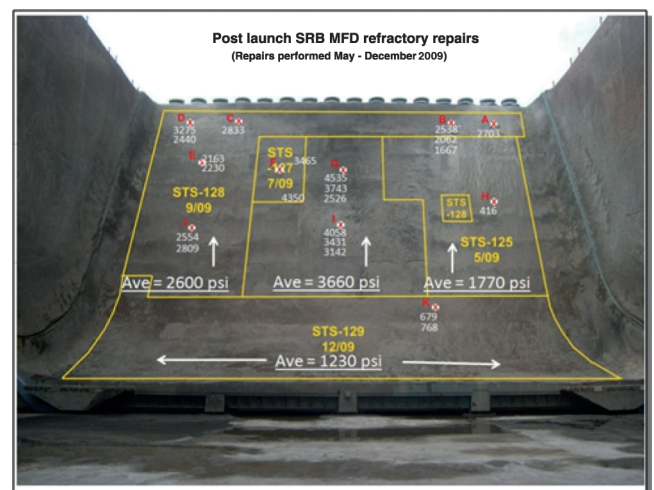
Fig. 2   Compressive strengths of refractory concrete on MFD.
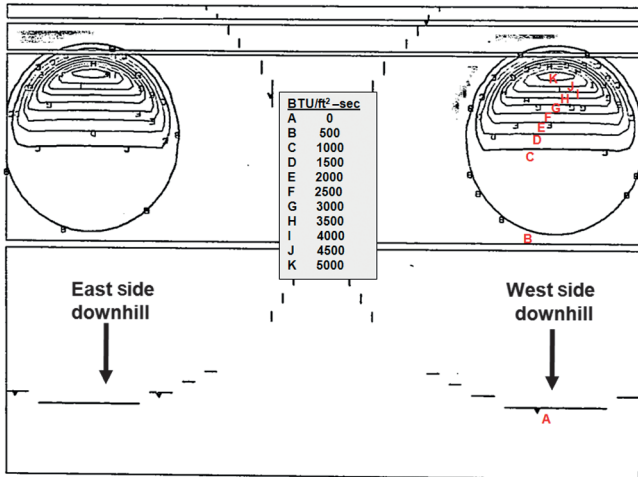
Fig. 3　Calculated GP-1059 heat rate contours on the MFD 1 s after SRB ignition (plan view).

Fig. 5　Final sensor installation before STS-134.

a pressure transducer was installed on the centerline of the MFD near the top because this location does not see direct plume impingement and measures acoustic pressure. The upper right corner of Fig. 4 shows the MFD sleeve penetrations, into which the sensors were inserted. These sleeves are approximately 3 ft apart. Figure 5 shows the final sensor installations. Notice the color of the cast refractory concrete along the right side and bottom apron of the MFD is different than the gunned concrete in the middle and to the left side of the MFD.

III.　Installed Instrumentation

A.　Commercial-off-the-Shelf Sensors

NASA has had a long, successful history of using COTS sensors in launch environments, including the studies on the side flame deflector and flame trench walls near the MFD. The intent of including the COTS products in the design is to provide comparative data to the tungsten piston, thus increasing the confidence in the measurement. Based on this experience, four types of sensors were procured to measure the plume's extreme environment. The following COTS sensors were used in the testing: a Medtherm® calorimeter (upper measurement limit: 4000 Btu/ft$^2 \cdot$ s), a Nanmac® erodible thermocouple (-191–$1414°$C), Kulite® or Stellar® pressure transducers (upper measurement limit: 300 and 200 psia,

respectively), and PCB® accelerometers (± 500 g). The PCB accelerometers were adhered to the backside of the MFD to measure vibration, and the data acquired from those transducers are not presented in this article. The Medtherms, Nanmacs, and Kulites or Stellars are installed in a 3-in.-diam 304 stainless cap screwed into a stainless housing. Figure 6 depicts the COTS assembly ready for installation.

The Medtherm calorimeter, shown in Fig. 7 before installation in the COTS cap housing, includes tubes for water, an independent type K thermocouple to measure its body temperature, and electrical leads for the heat rate measurement. All of these connections exit the backside of the housing and are connected to the ground measurement system-2 data acquisition system for LC-39A. Because the Medtherm body must remain below 400°F to accurately measure the heat rate, it is connected to a water cooling system.

The Nanmac is an erodible thermocouple. It is composed of layers of thermocouple metals that make electrical contact as erosion occurs. Small "whiskers" or slivers of metal make contact between the insulated layers of conductors. For STS-133, a type C Nanmac was installed. Because temperatures were not as high as anticipated, the last two launches employed type K Nanmacs for greater sensitivity to voltage output and higher-fidelity measurements. Figure 8 illustrates the layers of metals that erode and create a conduction path for voltage generation.

Kulite pressure transducers were installed for STS-133 and STS-134 with a switch to Stellars in the last flight, which can be compared in Fig. 9. Kulites were chosen for their ability to measure both dynamic and static pressures in the acoustic environment of the MFD.
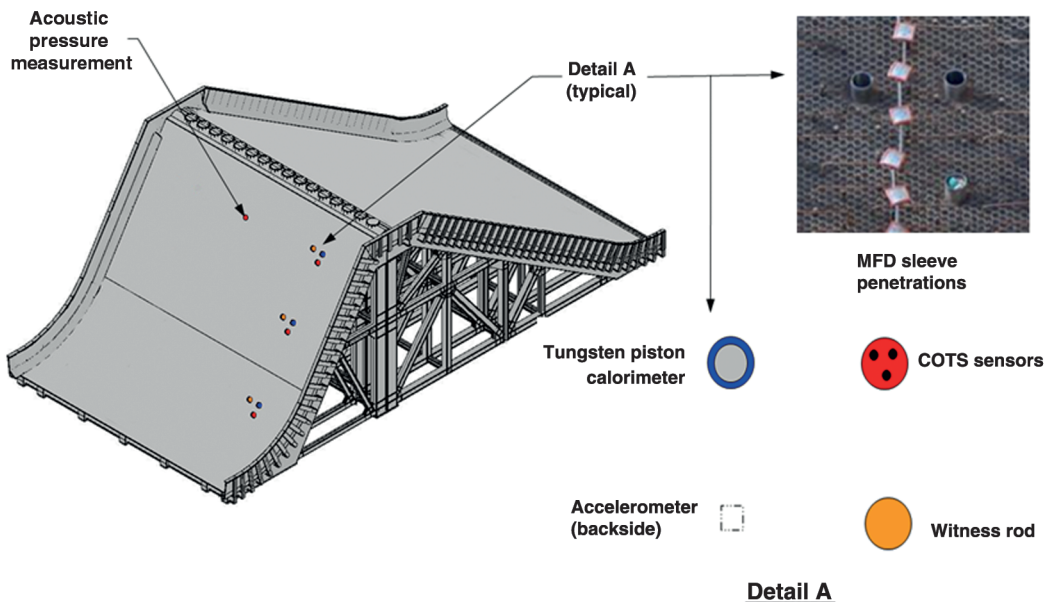
Fig. 4　Overall layout of sensors installed on the SRB side of the MFD.
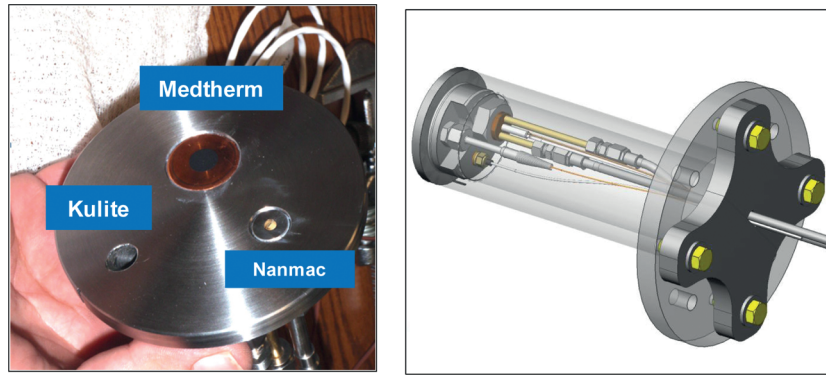
Fig. 6   COTS cap with sensors installed.

Fig. 7   Medtherm calorimeter.

Their frequency response of greater than 160 kHz in the expected pressure range allows capture of fast-changing pressure data, such as ignition overpressure. The Kulites accomplish this with a miniature Wheatstone bridge molecularly bonded to, but electrically isolated from, the miniature silicon diaphragm (integrated circuit technology). The silicon diaphragm is thought to be advantageous for resisting the high temperatures of the MFD environment. Review of the data after STS-133 and STS-134 shows false pressure increases after the main plume impingement. This data error is theorized to be

caused by thermal drift: the diaphragm of the Kulite heats up and expands, causing a change in resistance of the Wheatstone bridge that could be interpreted as pressure. This drift was eliminated in the last flight by using Stellar pressure transducers. The Stellars have a conventional stain gauge membrane that makes them heavier, more robust, and less sensitive than the Kulites. The added mass allows for more thermal energy absorption before thermal drift occurs. The tradeoff is that the frequency response for the Stellars is 1.5 kHz in the expected pressure range, which is a factor of 100 less responsive than the Kulites. The high natural frequency of the sensors, compared with the relatively low frequencies of the plume and structure, suggests that modal coupling between the transducers and their environment is not possible.

B.   Tungsten Piston Calorimeter

The launch environment is thermally severe and composed of molten aluminum oxide (AL_2O_3) being deposited on (or eroding) any structure in the flowfield. COTS sensors are not designed for this extreme environment, possibly causing them to erode or melt in the instant after SRB ignition. A robust sensor, the TPC, was developed to withstand the plume conditions and supplement the COTS data. Tungsten is used for its hardness and thermal properties. Of all the refractory metals it is the hardest (to resist erosion) and has the highest melting point (to resist the plume's heat). Its thermal diffusivity is similar to aluminum, making it an excellent thermal conductor. The TPC has three spring loaded thermocouples touching the bottom of thermal wells in the piston. This thermocouple installation is based on an experimental DLR (German Aerospace Center) rocket combustion chamber design [7]. The measured temperatures are used to back-calculate heat rates. The piston is connected via a rod to a load cell to measure the force of the plume on the piston.

Heat rates can be back-calculated by applying fundamental thermal equations to temperatures measured with respect to time and depth in the tungsten piston. Values obtained using this methodology can be directly compared with the Medtherm and are discussed in Sec. V. Similarly, pressures can be back-calculated by using the area of the piston surface and the load measured by a Strainsert load cell.
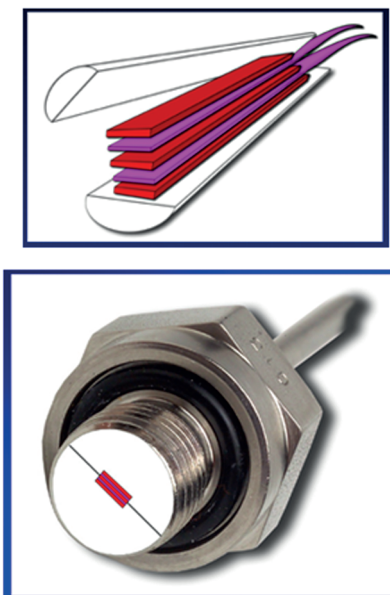
Fig. 8   Dissimilar metallic layers in the Nanmac thermocouple.

Fig. 9   Stellar (left) and Kulite (right) pressure transducers (not to scale).

Fig. 10   Insertion of thermocouples into a test article.

Values obtained by this calculation can be directly compared with the Kulite or Stellar pressure data. A high degree of confidence is given to measurements that correlate when acquired by more than one method.

The tungsten piston is a cylinder 3 in. in diameter by 3.5 in. long. Because of material availability and production costs, pistons were manufactured from both 99.99% pure tungsten and an alloy made of 90% tungsten, 6% nickel, and 4% copper. Three thermal wells 120° apart were electrical discharged machined in each piston from the bottom face (the cold side) to near the top (the hot face, exposed to the flame), leaving approximately 0.030, 0.060, and 0.090 in. of metal protecting the thermocouple tip from the plume environment. Type K 0.005-in.-diam thermocouples enclosed in two-hole ceramic tubes are shown in Fig. 10 being installed into the backside of a prototype steel piston. The depths of 0.030, 0.060, and 0.090 in. were chosen to ensure some thermocouples would survive if the plume significantly eroded the top of the TPC. After reviewing the data, tungsten is able to resist SRB plume erosion, and thermal wells as close to the surface as possible should be used in future applications.

Development testing, discussed in Sec. IV, shows that the tiny air gap between the type K metal thermocouple and the metal bottom of the thermal well causes significant resistance to conduction. The solution is to fill the air gap with a material that bonds to both metals, enhances conduction, and remains in place during the launch event. Figure 11 illustrates the difference in response of the thermocouples when the air gap is filled with a conductive metal. A heat rate of 500 Btu/ft$^2 \cdot$ s was applied to three differently installed thermocouples: bare-ended (with air gap), another with Field's metal, and one with SilFos® brazing. The Field's metal recorded the highest temperature, whereas the brazed thermocouple recorded the quickest rise in temperature, which is important in a short-duration event. Both offered superior performance over the thermocouple with the air gap. The Field's metal melting point at 144°F makes it easy to handle and install, but this material is repulsed by the tungsten and the type K thermocouple. Field's metal would melt and possibly vibrate free in the launch conditions, leaving only an air gap thermal path. The Sil-Fos easily wets both the thermocouple and piston and was selected as the material to form a permanent conductive pathway for the heat even when melted. The latent heat of fusion of the melting Sil-Fos is never observed in the launch temperature measurements because it is insignificant.

To braze the thermocouples, half of the weld bead of the thermocouple is removed with a grinding wheel under a microscope and replaced with Sil-Fos brazing. The remade thermocouple is then inserted into the well with a small amount of black flux, and a focused
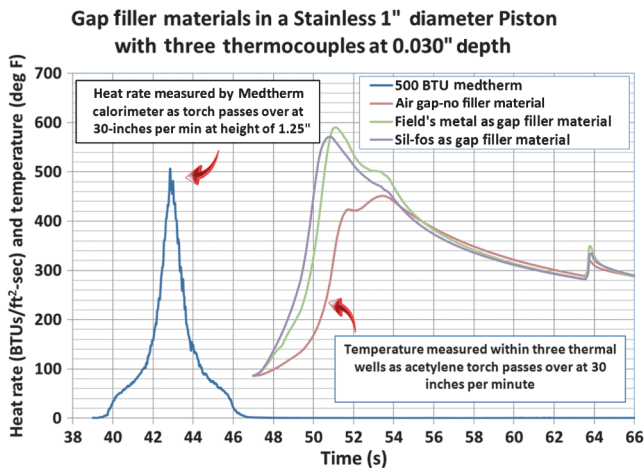
Fig. 11   The response of the thermocouples to gap-filler materials.
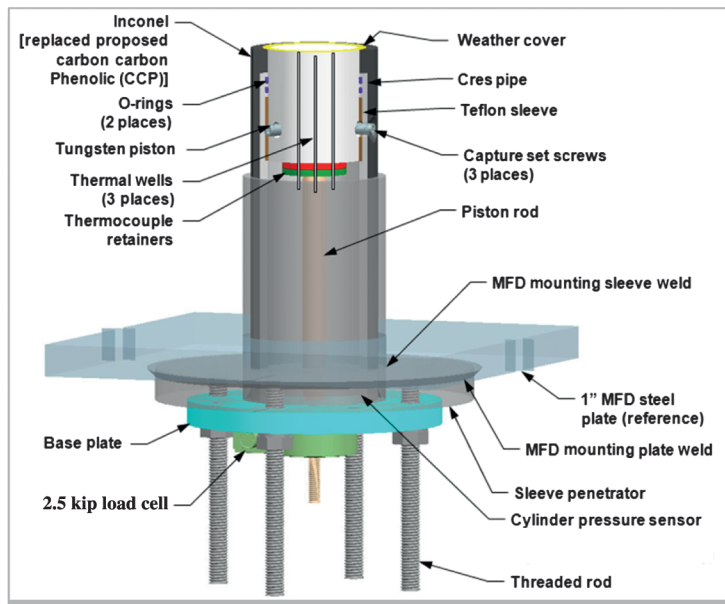
Fig. 12   The design and parts for the TPC.

Fig. 13   HY-80 witness rods ready for installation.

acetylene flame is applied to the hot face of the piston to melt the braze material. The temperature of the thermocouple is monitored to know when the Sil-Fos braze reaches its liquidus of 1200°F, causing the braze material to melt and permanently displace the air. A small spring is epoxied to the ceramic protective sheath to force contact between the metals while the piston is thermally expanding, but only a small amount of load can be applied without breaking the ceramic.

Figure 12 illustrates the details of the TPC. The tungsten piston is slid into a 304 stainless housing that contains double O-ring grooves to prevent plume blowby and a Teflon® bearing for the piston to ride on during plume lateral loading. This inner sleeve is installed in a sacrificial outer housing machined from either A-286 or 17-4PH stainless steel. To prevent direct thermal impingement of the plume on the upper O ring, three layers of 0.060-in.-thick high-temperature ceramic thread are packed into the gap between the piston and sleeve above the O rings. A rod connects the piston to a 2.5 kip Strainsert load cell to measure the total plume load. A Kulite pressure transducer is installed in the cavity beneath the piston in the event the O rings leak and hot gas partially pressurizes the cavity. If this occurs, a correction factor can be obtained to correct the plume pressure calculation for the difference between pressure on the top and bottom faces of the piston. The backside pressure (beneath the MFD)

remained close to ambient during the event, so no correction factor is needed. The electrical leads for the thermocouples, pressure transducer, and load cell leave the bottom of the sensor and are connected to the data acquisition system.

C.   Witness Rods

Witness rods 4 in. in diameter were installed in close proximity to the COTS and TPC sensors for each launch to qualitatively study the effect of the SRB plume on different steel types. 1018 steel was used for STS-134 because it is the material of choice for the exit cones of the SRB separation motors. HY-80 steel rods were installed for STS-133 and STS-135. HY-80 is used because of its high yield and tensile strength, good ductility, atmospheric corrosion resistance, and excellent weldability with reduced preheat. These qualities are desirable for an unprotected steel flame deflector if one were to be proposed for use in the future. The witness rods for STS-135 are shown ready for installation in Fig. 13.

IV.   TPC Validation Tests

During the development of the TPC, thermal, pressure, and vibration tests were performed to verify that the load cell and thermocouples would correctly measure the environment.

A.   Thermal Tests

The thermal tests validated both TPC fabrication methods and the numerical method used to calculate the heat rates from the thermocouple data. Aluminum, stainless steel, and tungsten test articles 1 in. in diameter were used. Over 50 tests were performed using an oxyacetylene torch as shown in Fig. 14a. The oxyacetylene torch was passed over the Medtherm and TPC to develop TPC fabrication methods and refine numerical methods for calculating heat rates from the thermocouples. Two Medtherm calorimeters (with maximum heating limits of 2000 and 500 Btu/ft$^2 \cdot$ s) were used to verify heat rates generated by the torch and to verify that the values each Medtherm measured were comparable. Sine wave and square wave heat profiles were applied to the prototype pistons and compared with the response of the Medtherms. The tests proved the importance of springs to hold the thermocouples tightly against
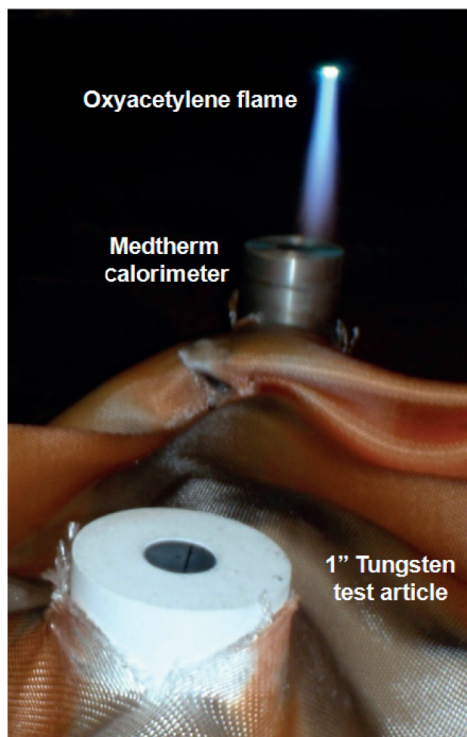
a) Thermal testing of the TPC
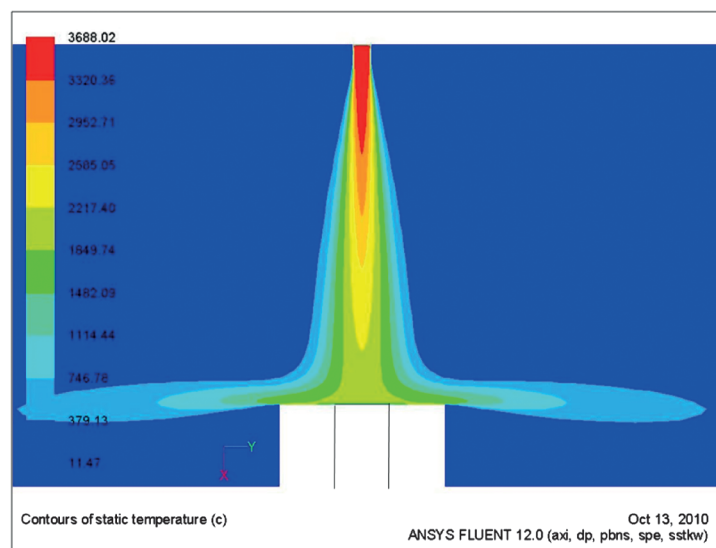
b) Modeled over a 1-in.-diam test article to determine 3D effects

Fig. 14   Oxyacetylene flame.

Fig. 15 Static leak check and dynamic response testing.

the bottom of the thermal well. Filling the air gap between the thermocouple and tungsten thermal well to produce a conductive pathway greatly improved the repeatability of the back-calculated heat rates. Finding the correct gap-filler material, as in Fig. 11, to "wet" the thermocouple and tungsten piston, as well as determining the correct procedure to braze the thermocouples to the bottom of the thermal well, proved to be two of the more difficult aspects in fabricating a repeatable sensor.

The TPC consistently calculated heat rates 20% less than those values measured by the Medtherms in the oxyacetylene tests. An ANSYS® Fluent model of the plume shown in Fig. 14b indicates that it is highly three dimensional (3-D). It was speculated that the small diameter measuring area on the Medtherm calorimeter (approximately 0.050 in. in diameter) was successful at measuring the pinpoint where the maximum heat rate occurs. It was also speculated that the large diameter TPC cannot perform as well with such a 3-D small diameter flame. However, when placed beneath a larger heat source (e.g., the 12-ft-diam SRB plume) it would function as expected. The measured SRB heat rates discussed in Sec. V support this assumption.

B. Pressure Tests

Pressure tests were divided into static leak checks and dynamic pressure spikes to compare the 2.5 kip Strainsert load cell to the 0–300 psia Kulite pressure transducer. The tests were performed by pressurizing a cavity above the piston as shown in Fig. 15. Leak check pressures (i.e., static pressures) were applied slowly and showed that the piston's O-rings held the internal pressure for the 10 min duration of the test. The load cell output was converted to pressure and was within 2% of the Kulite reading. To verify the load cell would track a
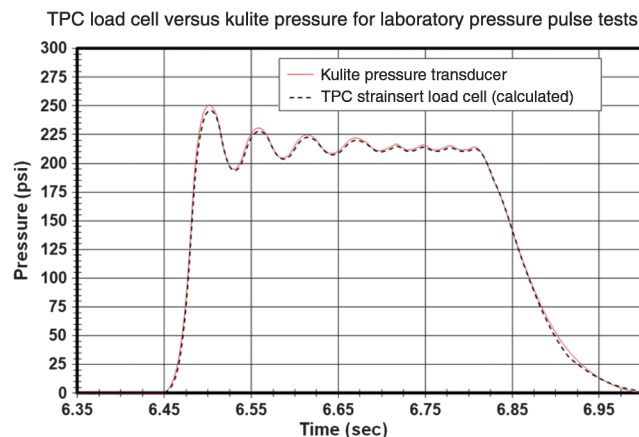
Fig. 16 Pressure test on piston/load cell system.

pressure spike similar to the SRB ignition overpressure, a dynamic pressure spike was generated by manually opening a valve in approximately 0.05 s. Figure 16 shows the response of the Strainsert load cell as compared with the Kulite pressure transducer. The piston/load cell tracked the pressure pulse within 5 psi on an amplitude pulse of 250 psi. This pressure oscillated within the closed cavity, creating a resonate frequency of between 10 and 25 Hz (depending upon the rapidness of valve actuation). These tests validated the similarity in response of the two pressure measurement methodologies.

C. Frequency Response Modeling and Vibration Testing

The structural load into the piston/load cell is a result of two input sources. The first is the transient input from the SRB plume directly, whereas a secondary load can occur from the dynamic response of the MFD, onto which the TPC is hard mounted, due to its response to the plume. A dynamic analysis was conducted using a finite element model (FEM) of the TPC mounted to the MFD. This analysis investigated the effects of the base excitation of the MFD on the TPC's ability to accurately measure the pressure of the direct SRB plume. The FEM is shown in Fig. 17. The force inputs [power spectral densities (PSDs)] are derived from the measured pressure and vibration environments, and these derivations are consistent with GSFC-STD-7000 [8]. The PSDs presented in Fig. 18 are calculated from both measured pressures on the bottom of the mobile launch platform (MLP) and measured accelerations on the backside of the MFD steel panels directly beneath the location of SRB plume impingement. Inspection of the PSDs shows that most of the pressure energy in the plume is below 40 Hz, whereas all of the peak responses of the MFD PSDs occur below 140 Hz. The FEM found the natural frequency to be approximately 300 Hz, a sufficient frequency separation.

Because it was determined that the effects of base excitation were negligible, the assembly was vibration tested to determine the natural frequency of the piston/load cell system and to ensure the structure would remain intact for three launches. Random and sine sweep vibration tests were performed in accordance with KSC-STD-164B, environmental test methods for ground support equipment [9]. The input PSDs were modified slightly to accommodate the Unholtz-Dickie shaker table's capabilities. The assembled TPC (with a steel piston) mounted to the Unholtz-Dickie during a vibration test is shown in Fig. 19. Figure 20 shows the response of several triaxial accelerometers installed on an axis aligned with the piston rod and
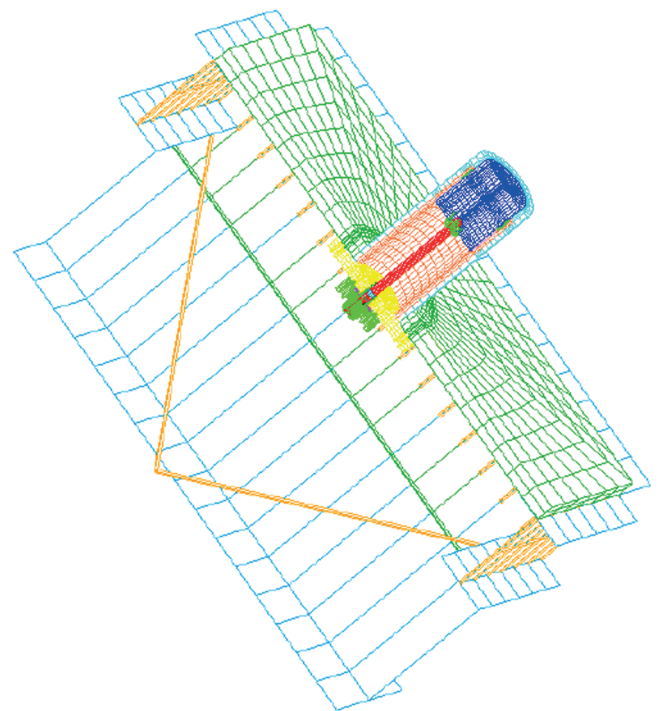
Fig. 17 FEM of TPC mounted in flame deflector structure.
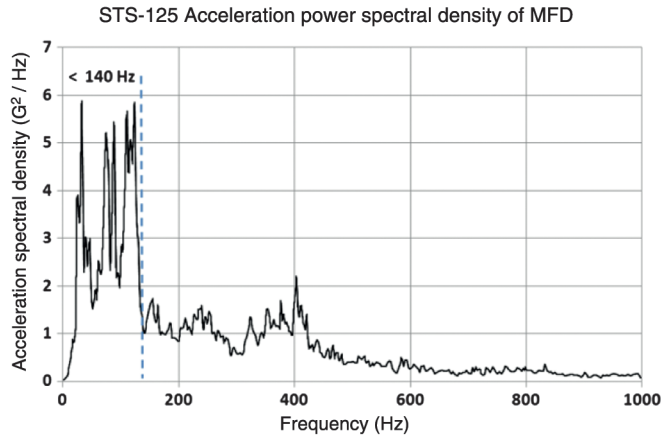
Fig. 18   STS-125 and STS-129 PSDs used as input for the FEM dynamic analysis.
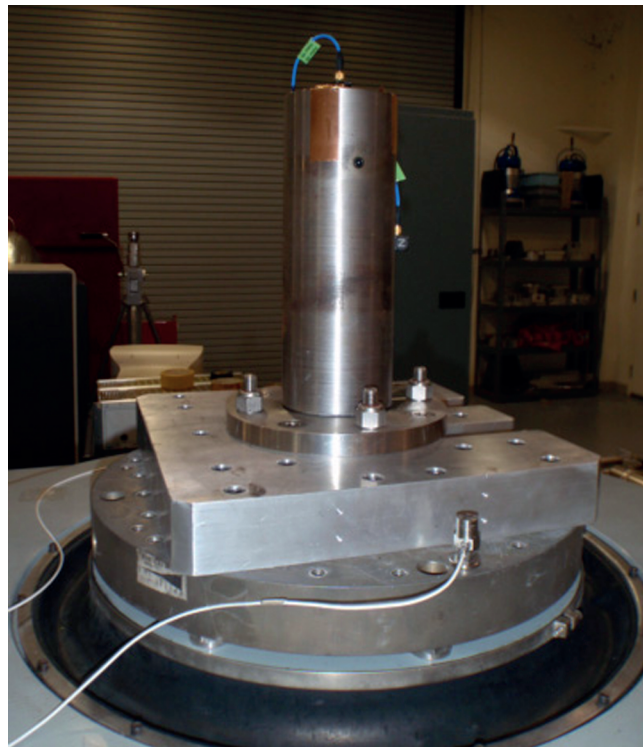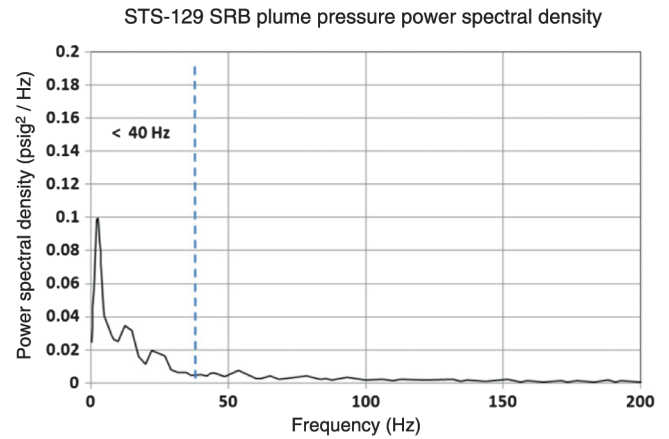
Fig. 19   TPC during vibration testing.

load cell. The sine sweep tests showed the resonant frequency of the piston/load cell subsystem to be 280 Hz. This is sufficient frequency separation that neither the plume's energy content below 40 Hz nor the MFD's frequency response of 140 Hz will excite the TPC. It was
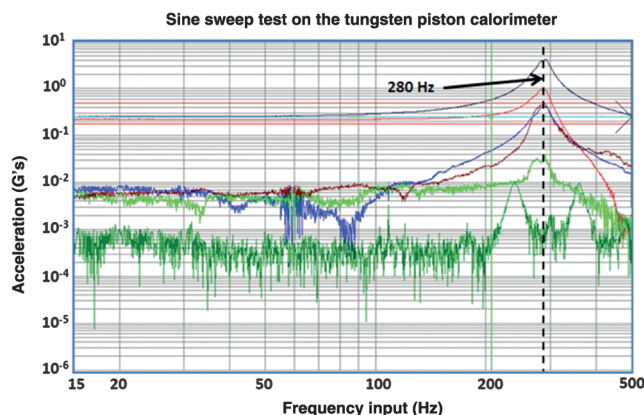
concluded that the piston should be dominantly loaded by the plume, and the filtered data presented support this conclusion.

V.   Results

A.   Plume Pressure

The pressure measurements from the Kulites and the Stellars returned similar pressure curves for the three launches. The peak values were over twice as high as those reported in GP-1059. Figure 21 compares Strainsert load cell and Stellar pressure transducer data for the three locations on the MFD for the last launch. To arrive at this summary, the raw data from the load cell and the Kulites and Stellars are processed to filter out the high-frequency acoustic and vibration signals. Raw data for the pressure transducers and load cell are recorded at 9600 Hz. The raw data are analyzed using Mathworks MATLAB® software's built-in *butter* and *filter* functions, which create a Butterworth lowpass filter set at 50 Hz. This limit is used because PSDs from previous launches identified that most of the plume's energy lies below 40 Hz. The filtered data are then averaged over 48 points (0.005 s) to reduce the number of data points to a manageable quantity without erasing any pressure events. As presented in Fig. 21, the data are time shifted to the right by 0.005 s because of the averaging algorithm. Finally, the processed Strainsert force data are divided by the area of the exposed piston surface (7.07 in.^{2}) to calculate pressure.

The pressure graph from STS-135 shown in Fig. 21 represents the only complete pressure measurement for an entire launch event. Thermal drift occurred in the pressures recorded by the Kulites installed for STS-133 and STS-134, indicating a loss of measurement accuracy later in the event (after the peak pressure occurred). There is high confidence that the peak pressures were successfully measured

Fig. 20   Resonate frequency of the TPC occurring at 280 Hz.
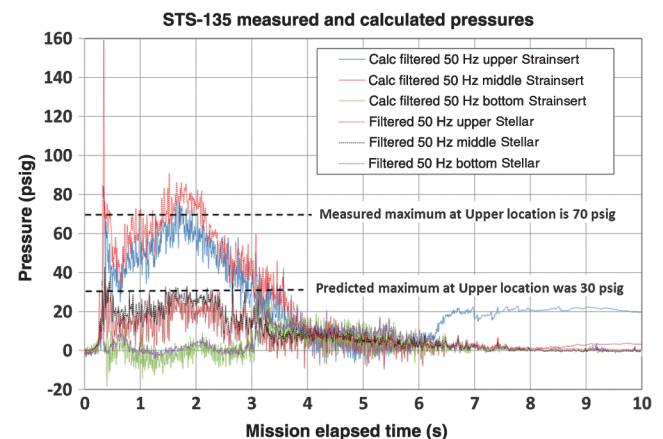
Fig. 21   STS-135 Pressures at the top/upper, middle, and lower sensor locations on the MFD.
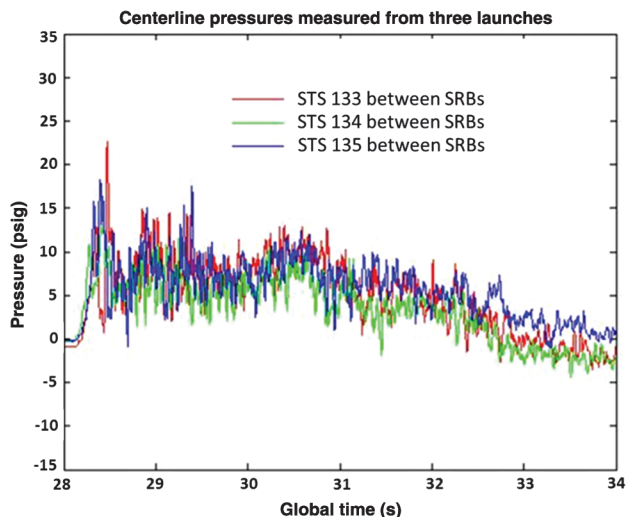
Fig. 22   Pressures measured on the MFD between two SRB plumes.

Fig. 23   Sound pressure measured during space shuttle launches [10].

for all three launches when these readings are compared with the Strainsert data.

Aside from the 160 psig short-duration ignition overpressure pulse that occurs around MET + 0.3 s, the maximum pressure recorded is over 70 psig on the STS-135 upper location. Upper locations for STS-133 and STS-134 using the Kulites recorded maximum pressures of around 60 psig. GP1059 cites a maximum pressure of 30 psig, a significantly lower value used as the historic design limit. The middle location, just 20 ft downhill from the upper, recorded the plume pressure decreasing by half and matches GP-1059's prediction. The bottom location records still lower pressures, as expected. Unexpectedly, between MET + 0.5 and 3 s, the bottom location measured negative pressures, indicating that the shape of the MFD surface, coupled with the Mach 2 plume, creates a partial vacuum. About 3 s after liftoff, the bottom location pressure increases to about 18 psig, indicating that the SRB plume is directly impinging on the lower MFD face as it traverses north during takeoff. These data show that pressures return to ambient around MET + 4 s, indicating the duration of the main launch event as it applies to the MFD structure.

B.   Acoustic Pressure

Acoustic pressure is primarily a consideration for payloads and ground support equipment. During the launch of STS-1, the reflected ignition overpressure pulse severely loaded Columbia's wings and control surfaces. One modification after STS-1 was the installation of water bags across the opening of the SRB engine exhaust holes to provide mass dampening for the reflected ignition overpressure pulse. Acoustic pressure had been measured as close as 10 ft above the SRB nozzle on the launch platform deck [10]. No measurements had been successfully taken below the MLP near the SRB nozzle exit plane. To gather a better understanding of near-field acoustic pressure, for the last three shuttle flights one Kulite pressure transducer was mounted on the MFD centerline, 55 ft below the exit plane, as shown in Figs. 4 and 5.

Figure 22 shows the peak acoustic pressure around 15 psig with a sustained average for 2 s of around 10 psig. The 15 psig peak pressure measured in this study is equivalent to a sound pressure of 194 dB, the theoretical maximum for nonshocked air. This is an increase over the linear acoustic law's prediction [11] (where linear acoustic laws are not valid below a 200 ft radius from the centerline of the rocket) and, as seen in Fig. 23, is much higher than measured by sensors closer to the nozzle but above the exit plane [10]. However, it is difficult to know how much pressure the plume contributes. Preliminary CFD studies performed at Marshall Space Flight Center [12] show plume pressure between 0 and 15 psig in the center region of the MFD, where the Kulite is installed. A more refined transient analysis is necessary to determine an exact pressure on the centerline to calculate
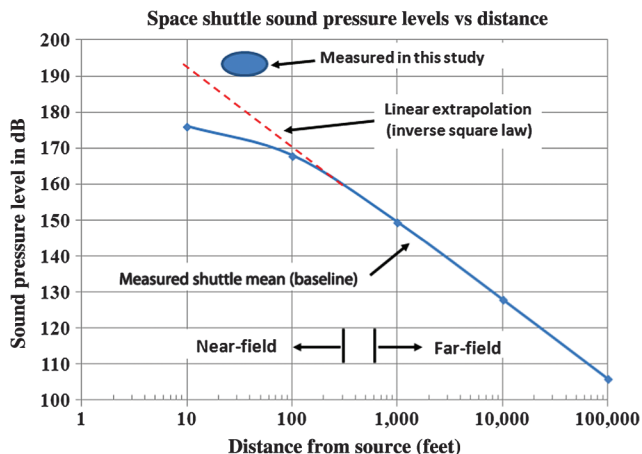
acoustic pressure and draw firm conclusions from the data gathered in this study.

C.   Temperatures

The Nanmac erodible thermocouples are installed flush with the surface of the COTS assembly cap and are exposed to the direct plume impingement. Directly measuring temperatures using this methodology is difficult considering that the top location did not record the complete event for any of the three launches, failing after MET + 0, 1.5, and 3.3 s, respectively. The middle location recorded the temperatures for the entire event for all three launches, whereas the lower Nanmac was successful for only STS-134 and STS-135. For much of the temperature rise in the first few seconds of launch, all three Nanmac locations experience similar temperatures. The maximum temperature recorded from any launch, 2160°F, occurs in the top location at MET + 3.24 s just before the thermocouple fails during STS-135, as seen in Fig. 24. Shortly after this time, the middle and bottom locations show decreasing temperature, and at the top location the slope of the temperature is not increasing when it fails, indicating temperature is not rising. Therefore, the maximum temperature of a complete top location data set is expected to be not much higher than 2160°F. This suggests that a boundary layer is protecting the Nanmac thermocouple (and MFD surface) when compared with GP-1059's predicted SRB plume temperatures of 4000°F. Factors contributing to the formation of the boundary layer include the sound suppression system water, the supersonic plume speed, and the undulations in the MFD surface.

The temperatures in Figs. 24 and 25 are graphed using raw data acquired at 1200 Hz. Before processing the TPC data with MATLAB to calculate heat rates, the data are smoothed with a 20-point running
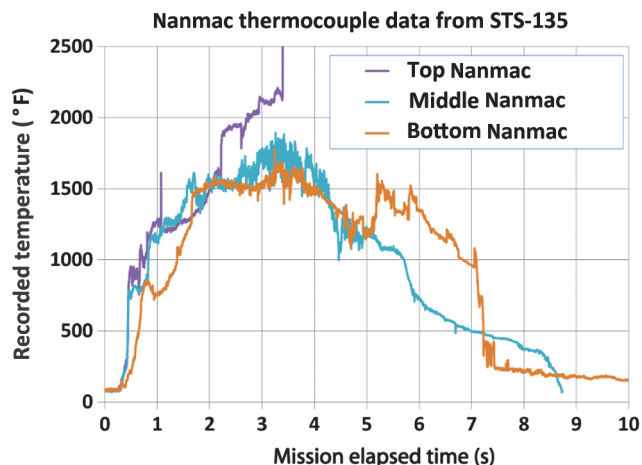
Fig. 24   Nanmac temperatures for top, middle, and bottom locations for STS-135.

average, illustrated in Fig. 26. Without this simple smoothing to minimize the signal noise, the calculated heat rates are hashy and unusable. The 20-point (0.0167 s) running average preserves the nuances in the temperature fluctuations and only minimizes the signal noise so heat rates can be accurately calculated.

Figure 25 compares the top Nanmac's temperature to the temperature profile within a tungsten piston. The temperatures are recorded by thermocouples inserted at distances approximately 0.030, 0.060, and 0.090 in. from the hot face of the piston. The magnitude of the Nanmac is similar to the uppermost 0.030 in. thermocouple, but the TPC records the temperatures at a delayed time. This illustrates the thermal diffusivity: the time it takes to conduct the plume heat through the solid tungsten to the thermocouples in the thermal wells. The heat rate calculation described in the subsequent section back-calculates a surface temperature from the depth of the thermocouple, accommodating for this apparent time delay. An inspection of the STS-135 calculated piston surface temperatures shows that the 0.030 in. thermocouple calculates a surface temperature close to the Nanmac values, but the deeper thermocouples calculate lower surface temperatures than measured. Interestingly, though it is close to the Nanmac in temperature, the STS-135 top TPC 0.030 in. thermocouple shown in Fig. 25 calculates out-of-family higher-energy content compared with other top location Medtherm and TPC thermocouples (see Table 1).

The 0.030 in. thermocouple in each piston was oriented uphill for STS-134 and STS-135. This thermocouple absorbs the majority of the three-dimensional and erosion heating. During launch, the aluminum oxide particles contained in the SRB combustion products scour the surface of the MFD. The particles significantly erode the leading edge of the piston housing sleeve. Piston sleeve erosion values can be found in Table 1. As the sleeve erodes, it heats due to
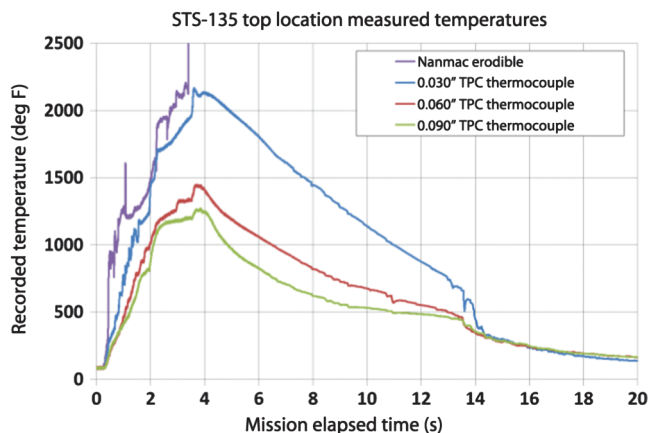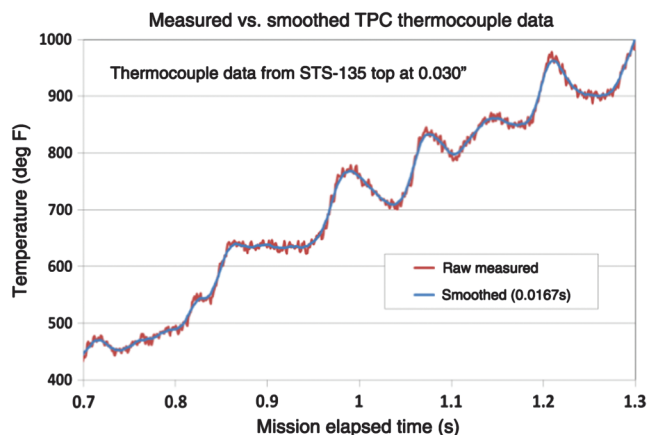
Table 1   Energy contained in heat rate profiles of each sensor with erosion amount

Heat Input into Each Sensor for 0–4.0 s (Btu/ft^2)				
Sensor/erosion	STS-133	STS-134	STS-135	Avg
Top				
Medtherm	1860	— —	2000	
TPC 0.030"	— —	— —	3140	2240
TPC 0.060"	— —	— —	2200	
TPC 0.090"	— —	— —	2020	
Piston sleeve erosion	0.189"	0.420"	0.205"	0.271"
Middle				
Medtherm	1360	1420	— —	
TPC 0.030"	1560	— —	2100	1660
TPC 0.060"	2200	1740	1520	
TPC 0.090"	— —	1760	1260	
Piston sleeve erosion	0.183"	0.236"	0.195"	0.205"
Bottom				
Medtherm	1040	940	940	
TPC 0.030"	780	1140	1080	960
TPC 0.060"	800	930	830	
TPC 0.090"	1300	— —	830	
Piston sleeve erosion	0.116"	0.146"	0.153"	0.138"

friction, heating the adjacent piston. Furthermore, as the sleeve erodes it exposes the leading edge of the TPC itself to the plume, described in Sec. V.E. This creates a 3-D heating situation and allows the temperature of the tungsten near the 0.030 in. thermocouple to increase faster than if it were top loaded only. A faster temperature increase results in higher calculated heat rates. The temperature should increase faster as the launch event continues and the piston sleeve erodes more. This does occur between MET + 2 and 4 s, in Fig. 25. Seen in Fig. 27, the heat rates resulting from this temperature increase are 30% higher than calculated by the other two thermocouples, which are less affected by 3-D heating. The temperatures recorded by the uphill thermocouples in all three locations appear to be artificially high.

D. Heat Rates

The TPC is a simple instrument with three thermocouples embedded at various depths near the heated surface of a tungsten cylinder. Heat rates are calculated from the measured transient temperatures using a numerical model that assumes one-dimensional heat flow into a 3.5-in.-long solid block with a known initial temperature. The piston surface temperature is calculated knowing the depth of the thermocouple, and the transient heat rate at the piston surface can be calculated using the thermal diffusion equation in Eq. (1). The material properties can be lumped together as thermal diffusivity α in Eq. (2). The material properties used are an average of the properties found during a literature survey for tungsten [13] and tungsten alloy.[**] The numerical solution only allows for constant properties, although they are found in the literature as a function of temperature:

$$\frac{\partial T}{\partial t} = \frac{k}{\rho c_v}\frac{\partial^2 T}{\partial x^2} \tag{1}$$

$$\alpha = \frac{k}{\rho c_v} \tag{2}$$

where for pure tungsten [13] $k = 80$ Btu/ft · h · °F, $\rho = 1203$ lb$_m$/ft^3, $c_v = 0.033$ Btu/lb$_m$ · °F, and $\alpha = 2.015$ ft^2/h.

The initial temperature condition is assumed to be a uniform ambient temperature, the average of the three thermocouples' data recorded before MET + 0 s. The back surface of the solid block is assumed to be adiabatic: a perfectly insulated surface where heat flow

Fig. 25   Nanmac and TPC thermocouples for the STS-135 top location.

Fig. 26   Averaging thermocouple data for processing.
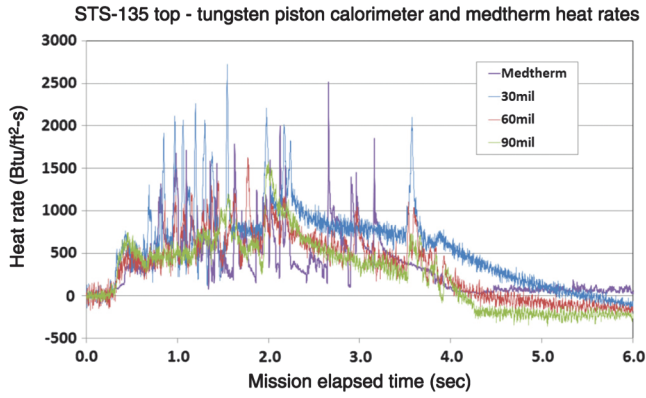
Fig. 27 The uphill (0.030 in.) thermocouple calculating a higher heat rate compared with the 0.060 and 0.090 in. thermocouples and Medtherm.

Fig. 29 Heat rates measured at the top location of 28% of the GP-1059 predicted value.

is defined as zero. According to a simulation of the piston using GP-1059 heat rates, during the short-duration launch event the heat will not penetrate to the back surface of the 3.5-in.-long tungsten piston, making it appear to be a semi-infinite thermal problem. In reality, any lost heat from the back surface would be negligible compared with the high heat rates on the hot surface. The measured thermocouple temperatures within the piston are used as the top surface boundary condition.

The desired surface heat flux is calculated from the time and space derivatives in the diffusion equation. The numerical model to solve Eq. (1) is programmed in MATLAB using a Gaussian substitution routine. A backward substitution using the adiabatic boundary condition produces the piston interior temperatures for the next time step. At each time step, the numerical solution back-calculates the surface temperature that causes the measured temperature reading. The measured thermocouple temperatures are used as the initial guess for the temperature of the surface node as the numerical solution iterates to calculate the surface temperature. The difference between the surface node (to which the measured temperature is applied) and the temperature of the node nearest to the specified thermocouple depth (at 0.030, 0.060, or 0.090 in. from the surface) is added to the surface node temperature for the next iteration. The temperature profile through the piston is recalculated, and the iteration process continues about 5–10 times until the temperature difference is minimal.

Further refinement of the algorithm is possible based on the assumptions made to develop the numerical solution, although these are minor corrections considering the many generalizations made in the algorithm. The constant temperature properties can be replaced with textbook temperature-varying properties. Because the thermal properties of tungsten vary among sources, the tungsten or alloy can be thermally tested to measure accurate properties for the particular hardware. The one-dimensional assumption simplifies the inherent 3-D nature of the block with thermocouple holes drilled into it. A
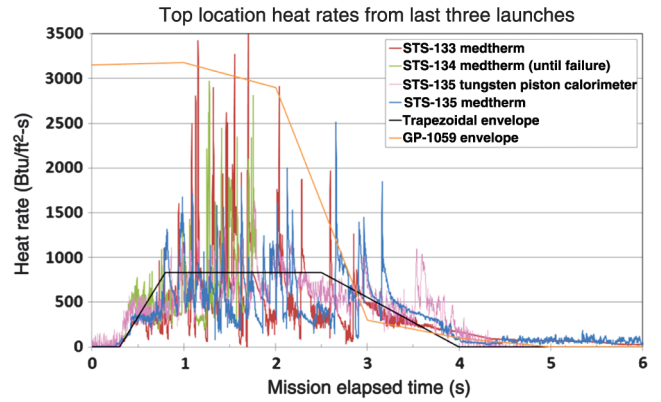
simulation of a piston with GP-1059 heat rates shows a small temperature variation across the bottom of the thermal well itself, where the thermocouple tip rests. The missing thermal mass causes a slight increase in thermal well temperatures, creating a 3-D effect, which could be modeled with the numerical solution.

Of the possible heat rate data sets from three TPC thermocouples and one Medtherm in each of three locations, STS-135 returned the most complete set of successful data without significant data dropout. Temperatures cannot be directly compared to determine environment temperature or heat rate. At greater distances from the hot face, the thermocouple will read lower temperatures, as in Fig. 25. Heat rate is a description of change in temperature, and the numerical solution adjusts for the depth of the thermocouple in its calculation. Sample heat rate profiles over the duration of the launch event are shown in Figs. 27–29 to compare the Medtherm vs TPC heat rate measurements. Qualitatively, the measurements are in-family, lasting about 4 s with heat rate spikes occurring at random intervals throughout the event. The qualitative difference between the sensor types is that the Medtherm is better able to record the quick spikes of heating. It has a smaller thermal mass and quicker response time. The TPC records some of these spikes, indicating they are real phenomena, but it is an instrument better suited to recording the general thermal energy content from the launch. To quantitatively compare the heat rate profiles, the measurements can be integrated to find the area under the curve, which is the energy per unit area that the plume imparts to the sensor. This integrated energy content summarizes the overall thermal effect of the launch on the MFD.

Because it is water cooled and remains at a constant temperature, the Medtherm records a cold-wall heat rate. As the TPC's surface temperature increases from 80 to 2000°F, the difference in temperature between the plume and the surface decreases. This decrease in temperature difference decreases the flow of energy into the piston, and consequently the calculated heat rates should be slightly lower than those measured by the Medtherm. The TPC hot-wall heat rates were never corrected to compare with the Medtherm
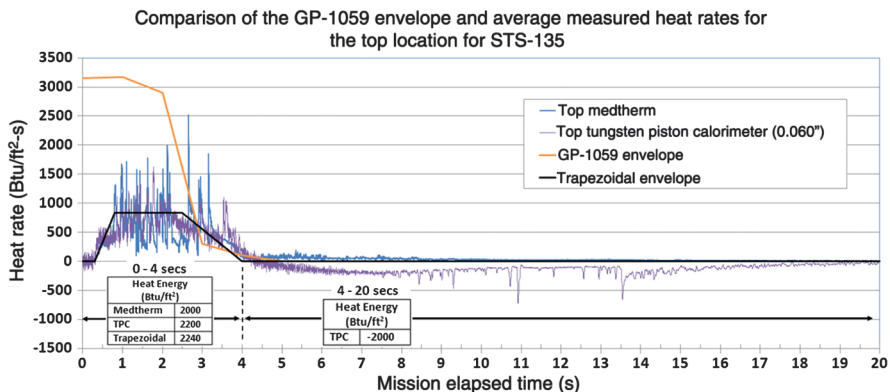
Fig. 28 Heat rate curves containing similar energy content versus GP-1059.
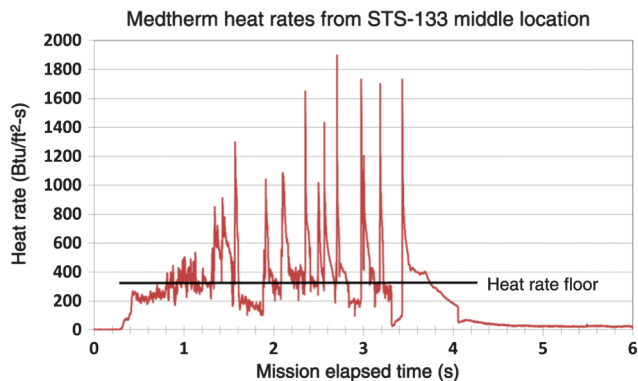
Fig. 30   Spikes in heat rate data compared with heat rate floor.

Fig. 31   Detailed profile of a heat rate spike, typical of each sensor and launch.

cold-wall heat rates. The results depicted in Table 1 show that even though the Medtherm heat rates were expected to be conservative they are in family with the TPC heat rates. The MFD surface behaves as a hot-wall system, and future designs can use the hot-wall heat rates without a problem.

Quantitatively, the Medtherm and TPC recorded similar heat rates. Samples of two heat rate profiles measured during STS-135 at the top location of the MFD are plotted in Fig. 28; the blue line is the Medtherm calorimeter and the purple line is the heat rate calculated from the TPC thermocouple at a depth of 0.060 in. Integrating over the entire 20 s of TPC data results in nearly zero energy transferred. The temperatures in Fig. 25 return almost to ambient when the data collection ends at MET + 20 s. The energy summaries listed on Fig. 28 show that the sum of the thermal energy into the piston in the first 4 s ($+2200$ Btu/ft^2) roughly equals the energy lost (-2000 Btu/ft^2) as the piston cools after launch, seen in the small negative purple spikes from MET + 4 to 20 s. The SRB travels far enough away from the MFD in the 4 s after SRB ignition that the sound suppression system water deluge can cover the surface of the TPC sensors and cool them quickly.

Inspection of Medtherm and TPC heat rate and pressure data from multiple launches shows that the majority of the MFD heating event is over by 4 s. Therefore, MET + 4 s is defined as the ending boundary for all mathematical integration to calculate thermal energy content. The temperatures recorded by the tungsten pistons shown in Fig. 25 have a negative slope after 4 s, meaning that the heat added to the piston by the plume has become small.

The areas under the heat rate curves of the Medtherm and TPC in Fig. 28, respectively, contain 2000 and 2200 Btu/ft^2 of heat energy input from launch. The trapezoidal-shaped black line in the figures contains 2240 Btu/ft^2 of energy, which is representative of the average energy content of all the sensors at the top location. Table 1 is a summary chart of the energy content into each sensor. The blue, purple, and black lines in Fig. 28 represent the same amount of energy. This simple trapezoidal profile illustrates how little energy is contained in the short-duration, high-heat-rate spikes. The total heat applied to the MFD in the trapezoidal profile is about 28% of the area under the orange curve, which is the heating predicted by GP-1059.

As illustrated by the orange lines in Figs. 28 and 29, GP-1059 publishes a heat rate that remains for the entire launch event at a magnitude similar to the heat rate spikes, describing an unrealistic situation with sustained high heat rates. The area under the GP-1059 curve contains 8000 Btu/ft^2, which is 3.5 times greater than the average heat content measured during three launches and illustrated by the trapezoidal profile. When first developed in the 1960s, this curve was likely based on the known heat of fusion of molten aluminum oxide ($\Delta H_f = 465$ Btu/lb$_m$) [14].

Why does GP-1059 describe an unrealistically high average heat rate? Examination of the thermal spikes acquired by the Medtherm/ TPC sheds light on the physical aspects of the plume. Data from the STS-133 middle Medtherm calorimeter are presented in Fig. 30 as an example of a typical heat rate profile. The plume is composed of a gas phase and aluminum oxide particles (or particle phase). These spikes are the accretion (or freezing) of the aluminum oxide slag onto the
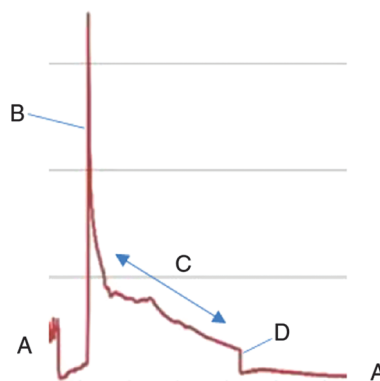
sensor. The curves indicate slag accretion, conductive heating, liberation, and erosion sequences during the plume impingement event, as described by the letters in Fig. 31, which is a detailed look at one spike from Fig. 30. The heat transferred to the substrate from the plume is constantly changing. The center of the impingement site on the MFD is approximately 55 ft from the nozzle exit plane at ignition. This distance allows the plume to expand and accelerate, causing the gas portion of the plume to cool. The particle portion of the plume, the Al$_2$O$_3$ particles (or "slag"), has a higher thermal mass and remains in the molten state before impinging on the MFD. The heat still contained in the slag is transferred to the substrate as the heating spike (B). The rapid reduction in heat rate (descent portion of the B spike and C) is the tapering off of the heat rate as the solidified slag in contact with the substrate cools through conduction. As the slag cools, it becomes more brittle. The MFD's vibration liberates the slag from the substrate, as seen by the rapid drop in heat rate (D) back to the "floor" (A). Once the protective layer of slag is liberated, the substrate is exposed to erosion and convective heating from the gas phase of the plume.

The heat rate floor identified in Fig. 30 (about 350 Btu/ft^2 · s) appears to be the same order of magnitude as the heat rates from the gaseous portion of the SRB plume, as presented in Figs. 7–15 in G P-1059 (600 Btu/ft^2 · s) [1]. In fact, all five successful Medtherm readings from the top and middle locations show a similar heat rate floor of 300–350 Btu/ft^2 · s. However, when integrating over the 4 s event, the top calorimeters measured a different energy content than the middle location, the additional energy coming from more slag impinging at the top. This is expected because the top location was directly beneath the plume at ignition. The spikes from the slag impingement correlate with the particle portion of the plume, as presented in Figs. 7–15 in GP-1059. Figure 29 shows that GP-1059 envelopes the slag spikes. The authors of that document did not have the advantage of actually measuring the short duration of the heat

Fig. 32   Scallops created by the SRB plume on the refractory concrete before the STS-133 refurbishment.

Fig. 33   Top TPC and housing after STS-135.
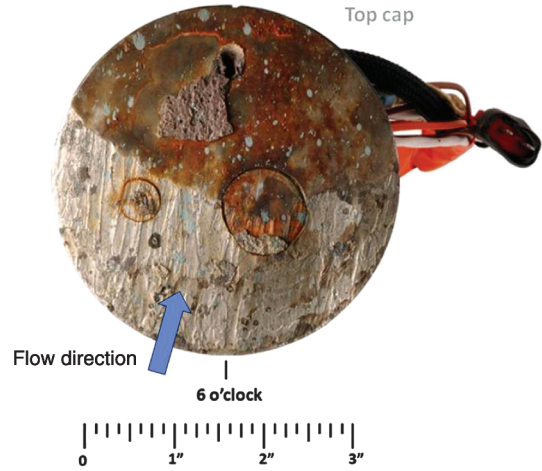
Fig. 34   STS-133 top COTS cap made of 304 stainless, sensors still installed.

loading from the spikes. Whereas the details of the heat transfer mechanism are open to interpretation, the overall energy can be summarized by the trapezoidal profile shown in Fig. 28.

E.   Witness Material Evaluation

Historically, the SRB plume erodes the refractory concrete, exposing the heads of the 1/2-in.-diam Nelson® studs to the environment. The studs are part of the mechanical system that holds the refractory concrete to the MFD. As discussed in Sec. II, during the MFD repair process many of these studs were removed and metallurgically examined to discover that melting of the steel did not occur [2]. This discrepancy suggested further investigation was valuable with larger diameter specimens. Three 4-in.-diam steel witness rods were installed in close proximity to the COTS and TPC sensors to gather qualitative data on the environment. The STS-133 and STS-135 launches exposed HY-80 steel to the plume, whereas the STS-134 launch exposed 1018 steel. In addition, other metals used for housing the TPC and COTS sensors (A-286, 17-4PH, and 304 stainless) were also examined. Pure tungsten pistons were used on STS-133 and STS-135, whereas tungsten alloy pistons made of 90% W-6% Ni-4% Cu were used on STS-134. The applicable material properties and the response of the various metals to the plume are summarized in Table 2. Only the responses of the witness materials for the top location are discussed because this location experiences the most severe thermal/erosive environment. A complete evaluation of the witness materials exposed to lesser heat rates in the middle and bottom locations on the MFD is covered in the references [15–17].

Table 2 indicates that thermal diffusivity [Eq. (2)] affects whether the material exhibits melting and/or erosion when exposed to the plume at the top location. Erosion values for all the steels, including the stainless, and the tungsten alloy were between 0.1 and 0.4 in. per launch. Steels with high thermal diffusivity did not melt, whereas the stainless steels with lower diffusivity did melt. Erosion of the steels

varies between launches, and there is no evidence that any type of steels eroded less than any other (even when considering that melting should cause an increase in erosion). The 99.99% pure tungsten installed in the top location exhibited a minimal amount of erosion. The erosive responses of the tungsten alloy and steel are similar, although their thermal diffusivities are not similar. The measured hardnesses of the pure and alloy tungsten pistons were similar, but for unknown reasons these materials displayed very different erosive responses.

Placement of the witness rods with respect to the undulations on the MFD explains why the erosion behavior is difficult to predict. The complexity of the boundary layer and formation of refractory concrete scouring ridges after multiple launches are shown in Fig. 32 (as photographed before the STS-133 MFD refurbishment). The scouring ridges highlighted by the shadows and sunlight are reminders of the severe turbulence within the boundary layer as the plume flows down the MFD surface. For this study, the west side of the MFD refractory concrete was initially smooth except for 0.5-in.-high casting ridges from the formwork, as discussed in Sec. II. The sensor arrays were installed flush with the surface of the MFD that had minor undulations as shown in Fig 5. After only three launches the beginnings of the scouring seen in Fig. 33 had started to appear.

Figure 33 shows the top tungsten piston and its A-286 stainless housing after the launch of STS-135. The housing displayed signs of melting: dendrites and distorted grain structure. An accompanying 0.2 in. of erosion occurred on the uphill side of the housing (to the right in the photo), whereas the piston showed no signs of erosion. This housing erosion exposed the leading edge of the piston to 3-D heating from the plume, as discussed in Sec. V.D. Slag is seen deposited on the piston and housing and in the groove between the piston and the housing. Whenever pure tungsten was placed in the top or middle locations, it cracked as shown in Fig. 33. This cracking

Table 2   Witness material properties and their response to the SRB plume for the top sensor location

Witness materials top location	Density, lb_m/ft^3	Specific heat, Btu/lb_m-°F	Thermal conductivity, $Btu/h \cdot ft \cdot F$		Thermal diffusivity, ft^2/h	Melting temp, °F	Response	Erosion, in.
Steels								
1018	490.8	0.116	30	——	0.527	2600–2800	Eroded	0.384
HY 80	483.8	0.11	22	——	0.413	2595	Eroded	0.079/0.225[a]
Stainless steels								
304	493.2	0.114	8.6@	80°F	0.153	2552–2642	Melted	0.244/0.340[b]
A286	494	0.11	8.7@	300°F	0.159	2550	Melted	0.189/0.205[a]
17–4ph	487.3	0.108	10.3@	300°F	0.196	2552–2624	Melted	0.42
Tungsten								
Pure (99.99%)	1203.1	0.033	84.4@	500°F	2.126	6192	Slight erosion	0.000/0.012[a]
Alloy (90%W-6Ni-4Cu)	1059.3	0.031	56.6@	500°F	1.724	5430–5790	Eroded	0.231

[a]For two launches.
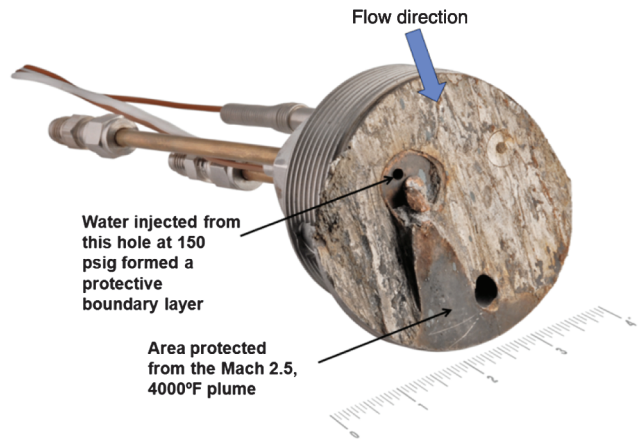
Fig. 35 STS-134 top COTS cap showing area protected by ejected water.

occurred from either the initial plume impingement or from the sound suppression system water rapidly cooling the piston after the event.

During STS-133, the top COTS cap made of 304 stainless eroded and melted a maximum of 0.244 in. on the leading edge, shown in Fig. 34. The Medtherm calorimeter survived the launch with minimal damage. In comparison, Fig. 35 shows the 304 stainless steel top COTS cap from STS-134, where the Medtherm was destroyed. Metallography showed that the 304 stainless melted and resolidified. Erosion was so severe that the water cooling lines on the Medtherm calorimeter in the COTS cap were exposed, as identified in Fig. 35. Water was injected into the atmosphere at 150 psig. This water formed a protective layer over the COTS housing downstream from the injection hole. This protection scheme is used by the Stennis Space Center B-1 space shuttle main engine test stand [18]. At that test stand, water is injected through numerous holes to protect the steel flame deflector from the space shuttle main engine exhaust. This finding suggests this thermal protection method could be considered for flame deflectors located beneath solid rocket motors during launch.

VI. Conclusions

A robust tungsten piston calorimeter (TPC) was successfully designed and fabricated to measure heat rates and pressures beneath the space shuttle solid rocket booster plume. Thermocouples brazed to the bottom of the piston's thermal wells produced a repeatable sensor with relatively fast response for heat rate calculations. Future designs of the calorimeter could embed the thermocouples even closer to the hot face of the piston. A load cell attached to the piston measured the plume pressure. A complimentary suite made from commercial-off-the-shelf (COTS) sensors performed better than expected in the harsh environment on the main flame deflector's face. The similarity in the data acquired from each sensor type indicates that heat rates and pressures were measured with a high degree of confidence.

The Medtherm calorimeter and the heat rates calculated from the change in TPC temperatures show that the ground support equipment environmental specification [1] overpredicts heating on the main flame deflector by a factor of three. The thermal spikes caused by the deposition of the aluminum oxide slag in the solid rocket booster plume were previously unidentified and measured by both the Medtherm calorimeter and the TPC. These spikes, although high in magnitude, add little energy to the heating of the main flame deflector in the plume.

Pressure data returned by both the load cell within the TPC and the COTS pressure transducers show that the specification [1] underpredicts maximum pressure by a factor of two. The data demonstrate that pressure and thermal loading from the launch event are over in about 4 s.

The data gathered in this study verified the anecdotal evidence that steel exposed to direct plume impingement does not melt. However

transient the event, no witness materials except pure tungsten were able to withstand the plume without some degree of mechanical erosion. Only metals with low thermal diffusivities have a propensity to melt; erosion is the only apparent damage mechanism to metals with higher diffusivities.

The modern approach for generating the environment at launch sites and test stands is to use computational fluid dynamics models. These models provide more apparent detail, but given the complicated nature of the flow and the assumptions required within the models their accuracy can only be determined by how they agree with measured data. This study acquired data at selected sites on the main flame deflector. Localized pressure, heat rate, and material response data can be used for realty checks at the location of the sensors in the models. In addition, the identifications of the short-duration thermal spikes and the measured heating profiles they generate are important findings that can be used when modeling the mechanism of slag deposition and liberation. All these models could be used for developing innovative thermal protection systems for future launch complexes and test stands.

References

[1] Murphy, W. T., "Environment and Test Specification Levels Ground Support Equipment for Space Shuttle System Launch Complex 39, Thermal and Pressure," NASA Engineering Development Directorate Rept. GP-1059, Vol. 4, Kennedy Space Center, FL, 13 April 1992, pp. 1–779.

[2] Salazar, V., "Failure Analysis of Main Flame Deflector Nelson Studs," NASA Engineering Directorate, Materials Science Div. Rept. KSC-MSL-2009-0297, Kennedy Space Center, FL, 2 Oct. 2009, pp. 1–7.

[3] Calle, L. M., Hintze, P. E., Parlier, C. R., Curran, J. P., Kolody, M. R., Sampson, J. W., and Montgomery, E. M., "Testing Requirements for Refractory Materials," NASA TM-2010-216293R, Feb. 2011, pp. 1–45.

[4] Anon., "Summary of Measurements of KSC Launch-Induced Environmental Effects (STS-1 Through STS-11)," Planning Research Corp. Rept. KSC-DD-818-TR, Kennedy Space Center, FL, June 1984, pp. 1–386.

[5] Clark, R. L., "Specification for Refractory Concrete," Kennedy Space Center Rept. KSC-SPEC-P-0012, 23 April 1979, p. 11.

[6] Sampson, J. W., "Properties of Refractory Concrete in Tension and Compression," NASA Engineering Directorate, Materials Science Div. Rept. KSC-MSL-2009-0336, Kennedy Space Center, FL, 13 Nov. 2009, p. 17.

[7] Suslov, D. I., Arnold, R., and Haidn, O. J., "Investigation of Two Dimensional Thermal Loads in the Region Near the Injector Head of a High Pressure Subscale Combustion Chamber," AIAA Paper 2009-450, 2009.

[8] Harper, A., Ryschkewitsch, M., Obenschain, A., and Day, R., "General Environmental Verification Standard (GEVS) For GSFC Flight Programs and Projects," NASA Goddard Space Flight Center Rept. GSFC-STD-7000, Greenbelt, MD, April 2005, pp. 1–151.

[9] Murphy, W. T., "Standard for Environmental Test Methods for Ground Support Equipment," NASA Engineering Development Directorate Rept. KSC-STD-164B, Kennedy Space Center, FL, 6 July 1992.

[10] Anon., "Far-Field Acoustic Environment Predictions for the NLS and Saturn V Derived Heavy Lift Launch Vehicles," Boeing Aerospace Corp. Rept. KSC-DM-3579, Kennedy Space Center, FL, March 1992, pp. 1–10.

[11] Arenas, J. P., and Margasahayan, R. N., "Noise and Vibration of Spacecraft Structures," *Ingeniare, Revista chilena de ingeniería*, Vol. 14, No. 3, 2006, pp. 251–264.
doi:10.4067/S0718-33052006000200009

[12] Mehta, M., Williams, B., Putman, G. C., and Smith, S. D., "Numerical Modeling of Solid Rocket Motor Plumes," *2012 TFAWS Aerothermal Session*, NASA Marshall Space Flight Center, Aug. 2012, p. 38.

[13] Yih, S. W. H., "Properties of Pure Metals: Tungsten," *Properties and Selection: Nonferrous Alloys and Special-Purpose Materials, ASM Handbook*, Vol. 2, ASM International, Russell Township, OH, 1990, pp. 1099–1201

[14] Gaskell, D. R., *Introduction to the Thermodynamics of Materials*, 4th ed., Taylor and Francis, New York, 2003, p. 587.

[15] Long, V., "Post STS-133 Evaluation of Main Flame Defector Witness Materials," NASA Engineering Directorate, Materials Science Div. Rept. KSC-MSL-2010-0344, Kennedy Space Center, FL, 6 July 2011, pp. 1–14.

[16] Long, V., "Post STS-134 Evaluation of Main Flame Defector Witness Materials," NASA Engineering Directorate, Materials Science Div. Rept. KSC-MSL-2011-0148, Kennedy Space Center, FL, 18 Nov. 2011, pp. 1–13.

[17] Long, V., "Post STS-135 Evaluation of Main Flame Defector Witness Materials," NASA Engineering Directorate, Materials Science Div. Rept. KSC-MSL-2011-0149, Kennedy Space Center, FL, 18 Nov. 2011, pp. 11–13.

[18] Sachdev, J. S., Ahuja, V., Hosangadi, A., and Allgood, D. C., "Analysis of Flame Deflector Spray Nozzles in Rocket Engine Test Stands," AIAA Paper 2010-6972, 2010.

G. Palmer
Associate Editor